

Physical Scale Modeling of VHF/UHF SAR Collection Geometries

C. Beaudoin^a, A. Gatesman^a, M. Clinard^a, J. Waldman^a, R. Giles^a and W. Nixon^b

^aSubmillimeter-Wave Technology Laboratory, University of Massachusetts Lowell,
Lowell, MA 01854 Ph: (978) 458-3807 Fax: (978) 452-3333

^bU.S. Army National Ground Intelligence Center, 2055 Boulders Road,
Charlottesville, VA 22911 Ph: (434) 980-7352 Fax: (434) 980-7999

Abstract- A method of physically modeling a linear flight path SAR collection in a scale-model VHF/UHF ISAR facility is presented. Accurate modeling of a SAR's collection geometry is necessary if meaningful comparisons are to be made between scale-model and field imagery. The advantage of collecting data in a linear flight path geometry is that height-unlimited focusing of scatterers can be achieved. The technique utilizes precise orientation of the target's azimuth and elevation relative to the fixed radar antenna, thereby effectively simulating a linear flight path collection. The impact of such a collection at VHF/UHF frequencies is demonstrated by comparing linear flight path ISAR imagery with traditional fixed grazing angle ISAR imagery. Both simulated and instrumented imagery will be presented.

I. INTRODUCTION

A VHF/UHF scale model radar signature collection technique has been developed that physically simulates a linear flight path (LFP) geometry in an indoor radar range environment. Typically, instrumented radar systems operate in a fixed grazing angle (FGA) ISAR mode and thus collect video phase history (VPH) data as a function of fast-time frequency and target azimuth [1,2]. From a polar format algorithm viewpoint, this type of ISAR collection locates VPH data on a section of a cone in the 3-D spatial frequency domain (SFD) [3-9]. Such a geometry imposes a limit on depth of focus for scatterers not located within a chosen focus plane. These scatterers will experience a phase error determined by their linear distance from the focus plane and the degree to which the collection surface in SFD deviates from a plane. If the VPH samples are collected in a planar slice of the SFD rather than on a conical surface, simultaneous focusing of volumetrically distributed scatterers is possible [3-6].

The degree of defocus is not significant for many operating bands where ISAR images are collected, so the FGA collection geometry is common. Because the azimuth aperture required for a given cross-range resolution (CRR) is proportional to wavelength, higher radar frequencies (e.g. X-

band) can obtain high CRR with relatively small ($<5^\circ$) angular apertures. Scatterers at different heights (e.g. foliage canopy, ground target) appear well focused in the resulting 2-D imagery. In addition, operating in the FGA ISAR mode allows rapid acquisition of target signatures for a full 360-degree range of target viewing angles without interruption of the collection process.

Wider angular apertures are required at the longer VHF/UHF wavelengths to achieve reasonable cross range resolution. The degree of defocusing becomes significant however, the more the collection surface deviates from a plane. The effects of such deviations from the ideal collection plane have been studied in detail [10]. Modeling a planar collection (or equivalently an ideal LFP) resolves the depth of focus problem resulting from the non-planar collection. However, there is some decrease in measurement throughput, because data for a full 360-degree range of target view angles cannot be collected continuously as in the FGA ISAR mode.

This paper outlines limitations in the depth of focus for VHF/UHF polar format imagery. This imagery is formed using VPH data collected with the FGA ISAR geometry and an indoor radar range-based LFP collection technique. The difference in imagery generated from LFP and FGA collections will be presented.

II. LIMITATIONS OF FIXED GRAZING ANGLE ISAR COLLECTIONS

Under the assumption of plane wave illumination and application of polar format processing [3-9], it can be shown that a FGA ISAR data collection geometry maps the VPH samples onto a conical surface in the 3-D SFD. To demonstrate this fact, the signal phase equation of a single point scatterer under plane wave illumination has been derived for a generalized ISAR collection geometry using a stepped frequency waveform. Fig. 1 illustrates the arbitrary data collection geometry depicting the relevant geometric parameters as well as the associated data format geometry in the SFD. Based on this generalized data collection geometry and plane wave illumination, the signal phase response of a point scatterer at (x_0, y_0, z_0) is:

Report Documentation Page			Form Approved OMB No. 0704-0188	
<p>Public reporting burden for the collection of information is estimated to average 1 hour per response, including the time for reviewing instructions, searching existing data sources, gathering and maintaining the data needed, and completing and reviewing the collection of information. Send comments regarding this burden estimate or any other aspect of this collection of information, including suggestions for reducing this burden, to Washington Headquarters Services, Directorate for Information Operations and Reports, 1215 Jefferson Davis Highway, Suite 1204, Arlington VA 22202-4302. Respondents should be aware that notwithstanding any other provision of law, no person shall be subject to a penalty for failing to comply with a collection of information if it does not display a currently valid OMB control number.</p>				
1. REPORT DATE APR 2004	2. REPORT TYPE	3. DATES COVERED 00-00-2004 to 00-00-2004		
4. TITLE AND SUBTITLE Physical Scale Modeling of VHF/UHF SAR Collection Geometries			5a. CONTRACT NUMBER	
			5b. GRANT NUMBER	
			5c. PROGRAM ELEMENT NUMBER	
6. AUTHOR(S)			5d. PROJECT NUMBER	
			5e. TASK NUMBER	
			5f. WORK UNIT NUMBER	
7. PERFORMING ORGANIZATION NAME(S) AND ADDRESS(ES) University of Massachusetts Lowell,Submillimeter-Wave Technology Laboratory,175 Cabot Street,Lowell,MA,01854			8. PERFORMING ORGANIZATION REPORT NUMBER	
9. SPONSORING/MONITORING AGENCY NAME(S) AND ADDRESS(ES)			10. SPONSOR/MONITOR'S ACRONYM(S)	
			11. SPONSOR/MONITOR'S REPORT NUMBER(S)	
12. DISTRIBUTION/AVAILABILITY STATEMENT Approved for public release; distribution unlimited				
13. SUPPLEMENTARY NOTES				
14. ABSTRACT				
15. SUBJECT TERMS				
16. SECURITY CLASSIFICATION OF: a. REPORT b. ABSTRACT c. THIS PAGE unclassified unclassified unclassified			17. LIMITATION OF ABSTRACT	18. NUMBER OF PAGES 6
19a. NAME OF RESPONSIBLE PERSON				

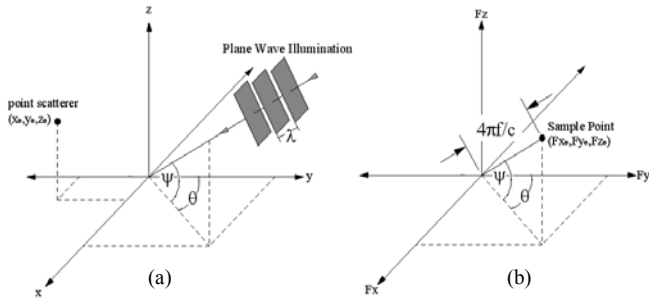


Fig. 1. Data collection (a) and format (b) geometries

$$\Phi(F_x, F_y, F_z) = e^{j(x_o F_x + y_o F_y + z_o F_z)} \quad (1)$$

$$F_x = \frac{4\pi f}{c} \cos(\psi) \sin(\theta) \quad (2)$$

$$F_y = \frac{4\pi f}{c} \cos(\psi) \cos(\theta) \quad (3)$$

$$F_z = \frac{4\pi f}{c} \sin(\psi) \quad (4)$$

Equations (1), (2), (3) and (4) describe the parametric mapping of the three Cartesian spatial frequency coordinates F_x , F_y and F_z , based on the collection parameters f , ψ , θ , and c the carrier frequency, grazing angle, azimuth angle, and speed of electromagnetic propagation, respectively. By eliminating the carrier frequency f and azimuth angle θ through successive substitution in (2), (3) and (4), the following equality can be derived:

$$F_z = \tan(\psi) \sqrt{F_x^2 + F_y^2} \quad (5)$$

Equation (5) demonstrates that if ψ is constant throughout the data collection, the VPH samples lie on a conical surface with vertex at the origin of the SFD.

In order to process the non-planar VPH samples resulting from a typical fixed grazing angle ISAR collection in a 2-D SAR image processor (i.e. polar format algorithm (PFA), backprojection, etc.), it is necessary to project the three-dimensionally distributed collection into a selected processing plane (e.g. the nominal slant or ground plane). The *direction* by which the data are projected into the processing plane defines the plane in which scatterers will be focused [3-6]. This plane, referred to as the focus target plane (FTP), is not necessarily the same as the processing plane. It is the projection from a curved to planar surface that limits the focusing of volumetrically distributed targets to a single plane. Planar collections do not suffer from such defocusing issues and can simultaneously focus all volumetrically distributed

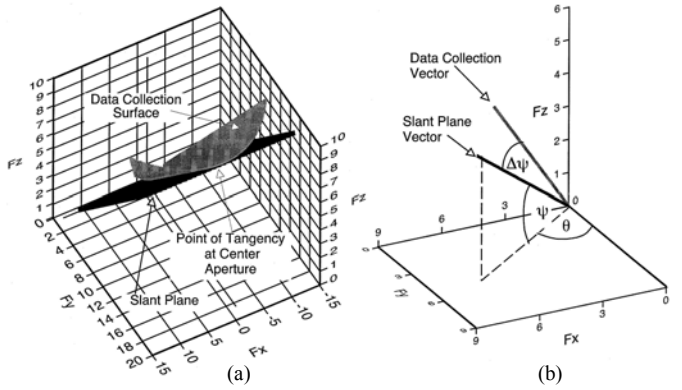


Fig. 2. Diagram of the conical FGA ISAR data collection surface and ideal slant plane in the SFD (a), and the data collection vector and ideal slant plane vector at a given azimuth angle ' θ ' (b). Note that in (b) $\Delta\psi = 0$ when $\theta = 0$ as indicated in (a)

scatterers. In the FGA data presented here, the VPH samples are projected to the processing (slant) plane in the $-F_z$ direction, thus defining the x - y (ground) plane as the FTP. Therefore, in imagery of the nonplanar FGA data all scatterers placed on the ground plane will appear well-focused and any scatterer that does not reside on the ground plane will appear defocused.

The defocusing caused by a nonplanar collection arises from an injection of quadratic phase error into the scatterer's phase response [3, 4] and is:

$$\Delta\phi = \frac{4\pi}{\lambda} \frac{\Delta\psi}{\cos(\psi_o)} \Delta h \quad (6)$$

Equation (6) quantifies the amount of phase error $\Delta\phi$ that is injected into the scatterer's phase response due to the scatterers differential height Δh out of the FTP and the differential grazing angle $\Delta\psi$ out of the selected ideal slant plane for a given center aperture grazing angle ψ_o . In the case of a FGA ISAR collection ψ_o is the fixed grazing angle.

By specifying a maximum amount of phase error $\Delta\phi$ that may be tolerated to generate focused imagery, the depth of focus (DOF) can be defined. The DOF is the value Δh that will induce the maximum tolerable phase error based on the center-band wavelength, differential grazing angle and center aperture grazing angle [3]. A typical limit on tolerable phase error is $\pi/4$ radians as this broadens the mainlobe width of the impulse response function by approximately one mainlobe width [3]. Whereas the center-band wavelength and center aperture grazing angle are easily ascertained from the imaging situation, the differential grazing angle must be derived based on a selected ideal slant plane. Traditionally this slant plane is taken as that tangent to the data collection cone at the central chirp of the collection aperture. The data format geometry demonstrating the relationship between the collection surface and the selected slant plane is shown in Fig.

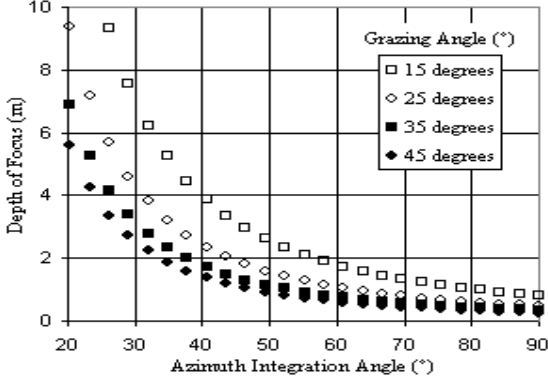


Fig. 3. 300 MHz FGA ISAR depth of focus plot at various grazing angles

2. A formulation of the differential grazing angle between the collection surface and the selected slant plane at azimuth angle θ can be developed by applying simple trigonometric principles based on Fig. 2:

$$\Delta\psi = \psi_o - \psi(\theta) = \psi_o - \tan^{-1}[\cos(\theta)\tan(\psi_o)] \quad (7)$$

Here, $\psi(\theta)$ describes the variation of the slant plane vector's grazing angle as a function of the azimuth angle. It can be shown that this variation in grazing angle is synonymous with that exhibited in an ideal linear flight path collection for which the broadside grazing angle is ψ_o . By implementing (6) and (7), the depth of focus may be quantified for the FGA ISAR collection. Fig. 3 quantifies the depth of focus parameter, as calculated by (6), between 20° and 90° azimuth integration for $\psi_o = 15^\circ, 25^\circ, 35^\circ$ and 45° at center-band frequency 300 MHz. As shown in Fig. 3, the depth of focus degrades with increasing azimuth integration angle, indicating that larger angular integrations will incur more phase error and therefore more defocusing for a given Δh . Also to be noted is the reduced depth of focus with increasing grazing angle. Based on Fig. 3, it is clear that if focusing of scatterers 3 meters or more out of the FTP is a requirement (as for foliage penetration radar studies), a FGA ISAR collection with a 30° grazing angle and 40° integration angle will not provide well-focused imagery.

III. ISAR MODELING OF PLANAR VPH COLLECTIONS

In order to overcome the depth of focus issue resulting from FGA ISAR collections, a planar VPH collection is required. Such a collection may be modeled in an indoor ISAR facility utilizing a mechanical turntable having both azimuth and grazing angle positioning capability. Insight as to how the azimuth and grazing angles must be synchronized for the case of a broadside collection is provided in (7), which describes the required grazing angle position ψ_s as a function of azimuth angle θ to synthesize a planar VPH collection:

TABLE I
Parameters of Simulated and Instrumented ISAR VPH Collection

Center Frequency	342 MHz
Bandwidth	342 MHz
Center Aperture Azimuth Angle θ	0° (Broadside Collection)
Azimuth Integration Angle (Span of θ)	90°
Nominal Grazing Angle ψ_o	30°
# Frequency Samples	102
# Aperture Samples	46

$$\psi_s = \tan^{-1}[\cos(\theta)\tan(\psi_o)] \quad (8)$$

This variation in grazing angle ψ_s over the synthetic aperture will map the VPH samples onto the slant plane in the SFD and will allow focusing of volumetric scatterers in subsequent ISAR image processing.

IV. ISAR IMAGERY OF SIMULATED PLANAR AND FGA VPH COLLECTIONS

To demonstrate the fidelity of the image formation processor (IFP) as well as the depth of focus issue from a theoretical perspective, ideal-point-scatterer-simulated ISAR VPH collections were generated under the assumption of plane wave illumination. In this paper, we refer to an ideal point scatterer as one which does not exhibit frequency, angle, or polarization dependence on scattering amplitude and/or phase. Fig. 4 shows the spatial distribution of the two point scatterers used in the simulation and Table I contains the relevant parameters used in the simulation. These parameters were chosen based on the capabilities of the scale-model ISAR measurement system.

Fig. 5 displays ISAR imagery of simulated VPH data collected using the FGA and planar geometries, respectively. The simulated data were processed using the polar format algorithm, defining the point of rotation in the x-y (ground) plane as the motion compensation point. The nonplanar FGA collection required that the VPH samples be projected to the processing (slant) plane in the SFD as outlined in the previous section. Both the FGA and LFP data were then interpolated from a polar to rectangular region of support in the SFD. A 2-D FFT routine was then applied to the interpolated data samples to generate the imagery displayed in Fig. 5. Aperture weighting was not applied to the interpolated data samples prior to Fourier inversion.

It should be noted that in a real-world UWB radar system capable of integrating over such a wide range of angles that the concept of an ideal point scatterer is strictly a mathematical ideality. However, this concept serves as a useful metric in demonstrating the merit of the IFP as well as the fundamental concepts described here. For brevity, we forego

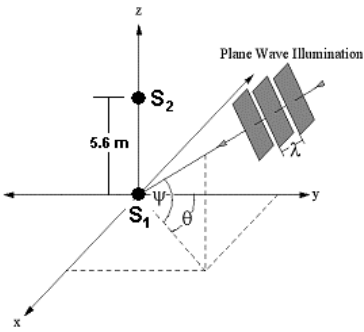


Fig. 4. Spatial distribution of point scatterers S_1 and S_2 used in simulated and instrumented collections

an in-depth performance analysis of the IFP [4] but point out that the imagery of the simulated point scatterers in Fig. 5b takes the form of the 2-D sinc function. This 2-D sinc function is characteristic of an unweighted ideal point scatterer phase response having a rectangular region of support in the SFD [3, 4].

Imagery of the simulated point scatterers demonstrates the depth of focus issue associated with the nonplanar FGA collection (Fig. 5a) and the resolution of this problem when a planar collection is employed (Fig. 5b). In Fig. 5, Scatterer S_1 appears at the origin of the image due to the fact that it is located at the motion compensation point. Due to the fact that scatterer S_2 is directly above S_1 and is not located in the ground plane, it experiences layover in the direction of the radar, appearing in front of scatterer S_1 in the images. In Fig. 5a, S_2 experiences defocusing due to the fact that the collection was nonplanar and it is not located in the focus plane. As a result of the planar collection, both scatterers S_1 and S_2 appear focused in the images displayed in Fig. 5b.

V. ISAR IMAGERY OF INSTRUMENTED PLANAR AND FGA VPH COLLECTIONS

To replicate the above simulation as closely as possible using a scale-model instrumented ISAR system, two trihedral corner reflectors were selected to model the point scatterers S_1 and S_2 in Fig. 4. The indoor ISAR system operated over the 6 – 18 GHz frequency band in HH polarization. When using 1/35th scale targets, the system models a full-scale radar system operating with center frequency 342 MHz and an equivalent bandwidth of 342 MHz. The dimensions of the trihedrals used in the experiment were on order of 1.4 in., modeling 4 ft. corner reflectors in full-scale dimensions. The ISAR system also possessed the required mechanical stages providing the necessary positioning of the target under measurement to perform planar and FGA collections. A description of the scale-model ISAR measurement system can be found in the literature [11]. The instrumented VPH data were collected using the same parameters in Table I. Imagery of the instrumented data was formed utilizing the same IFP incorporated in the simulated example.

Fig. 6 displays the imagery generated from the instrumented VPH data using the FGA and planar collection geometries, respectively. In comparing Fig. 5b and Fig. 6b, it is clear that the scattering centers of the imaged corner reflectors do not perfectly model their counterparts in the imagery of the simulated data. This discrepancy is due to the relatively simple ideal point scatterer model employed in the simulation. As we previously stated the ideal point scatterer is a mathematical ideality. The actual scattering behavior of a corner reflector is much more complex due to the widebandwidth signal and large aperture used to form the imagery. Despite the non-ideal point scattering behavior exhibited by the corner reflectors, the underlying principles regarding the relationship between the SAR collection geometry and image depth of focus is well demonstrated.

In comparing Fig. 5 and Fig. 6 it is obvious that the same image layover and defocusing effects discussed in the simulated example are observed in the instrumented example. As observed in Fig. 6a, imagery of the instrumented data collected using the FGA geometry displays defocusing of scatterer S_2 . This is due to the fact that the collection was nonplanar and S_2 was not located in the focus plane. Fig. 6b demonstrates that imagery of the planar-collected/instrumented data resolves the depth of focus problem inherent in a nonplanar collection. The advantage of collecting VPH data in a plane, equivalent to a linear flight path, is to achieve height-unlimited focusing of scatterers in the image reconstruction. It has therefore been demonstrated that physically modeling such a collection in a scale-model ISAR measurement system is possible.

VI. SUMMARY AND CONCLUSIONS

Through the use of simulated and instrumented data collections, we have demonstrated the capability of modeling a planar or linear flight path collection geometry in a scale-model ISAR facility. Imagery formed utilizing polar formatting served as the basis for this verification. Inherent defocusing effects due to planar and nonplanar collections were discussed and verified through imagery of simulated collections. Imagery of instrumented planar and nonplanar collections modeling the simulated data were then presented. Instrumented imagery was shown to exhibit the same defocusing effects of the simulated imagery, verifying that it is possible to model a linear flight path geometry with laboratory techniques.

The polar format algorithm and its properties were used in this work as a means to demonstrate the capability of physically modeling planar collection geometry. Polar formatting was the chosen imaging method as it accommodates turntable ISAR measurements due to the fact these measurements are inherently motion compensated to a point. This is not to say that polar formatting is the only method in which the data may be processed into imagery. Methods such as the range migration algorithm, which utilize a line motion compensation scheme, may also be used to process the instrumented data. This method would require the application of range shifts to the instrumented data on a chirp

by chirp basis to effectively convert the motion compensation scheme from that of a point to a line. Furthermore, it should also be noted that it is possible to model any arbitrary collection geometry in the indoor radar range with knowledge of the collection path.

As indicated, the main goal of this work was to provide a meaningful comparison between VHF/UHF scale-model and field SAR imagery. However, neither the field radar's antenna pattern nor the radar's changing slant range to the scene center were discussed. This is due to the fact that the model assumed the target was uniformly illuminated at all frequencies and at all positions of the SAR platform. While this is a valid assumption in the indoor radar environment, it is typically not valid in a field SAR collection. However, these antenna pattern/varying slant range effects must be rectified when field data is image processed to avoid image distortions. Therefore, in a comparison of scale-model and field measurements it is assumed that these effects have been removed during the image formation process. In the event that we may not assume that these effects have been removed, there is an alternative. With knowledge of the antenna's radiation pattern and the SAR's flight path, it is conceivable that the antenna pattern/varying slant range effects may be modeled mathematically and incorporated into the scale-model measurements. This is a topic of future research.

REFERENCES

- [1] R.H. Giles, W.T. Kersey, M.S. McFarlin, H.J. Neilson, R. Finley and W.E. Nixon," Target Variability and Exact Signature Reproduction Requirements for Ka-Band Radar Data," *Proceedings of the SPIE*, Vol. 4380, pp. 117-126, August 2001.
- [2] M. Coulombe, J. Waldman, R. Giles, A. Gatesman, T. Goyette, and W. Nixon, "Submillimeter-Wave Polarimetric Compact Ranges for Scale-Model Radar Measurements," *2002 IEEE MTT-S International Microwave Symposium*, Vol. 3, pp. 1583-1586, June 2002.
- [3] J.C.V. Jackowitz, D.E. Wahl, P.H. Eichel, D.C. Ghiglia, and P.A. Thompson, *Spotlight-mode Synthetic Aperture Radar: A Signal Processing Approach*. Norwell, MA: Kluwer Academic Publishers, 1996.
- [4] W.G. Carrara, R.S. Goodman, and R.M. Majewski, *Spotlight Synthetic Aperture Radar*. Norwood, MA: Artech House Inc., 1995.
- [5] J.L. Walker, "Range-doppler imaging of rotating objects," *IEEE Trans. Aerospace & Electronic Systems*, vol. 16, no. 1, pp. 23-52, Jan. 1980.
- [6] R. Lipps and D. Kerr, "Polar reformatting for ISAR imaging." *Proceedings of the 1998 IEEE Radar Conference*, pp. 275-280, May 1998.
- [7] Y.Yuan, J. Sun, and S.Mao, "PFA algorithm for airborne spotlight SAR imaging with nonideal motions," *IEE Proceedings- Radar, Sonar and Navigation*, vol. 149, issue 4, pp. 174-182, August 2002.
- [8] N.J.S. Stacy, "Synthetic aperture radar out of slant plane motion compensation," *IEEE 1997 International Symposium on Geoscience and Remote Sensing, IGARSS 1997*, vol. 2, pp. 728-730, Aug. 1997.
- [9] N.J.S. Stacy, "Range cell migration in the spotlight SAR polar format algorithm," *IEEE 2000 International Symposium on Geoscience and Remote Sensing, Proceedings. IGARSS 2000*, vol.5, pp. 2275-2277, July 2000.
- [10] D.R. Kirk, R.P. Maloney and M.E. Davis, "Impact of platform motion on wide-angle synthetic aperture radar (SAR) image quality," *The Record of the 1999 IEEE Radar Conference*, pp. 41- 46, April 1999.
- [11] C.J. Beaudoin, A.J. Gatesman, R.H. Giles, J. Waldman, M.E. Testorf, M.A. Fiddy, and W.E. Nixon, "A Foliage Penetrating Radar Imaging System," SPIE's 48th Annual Meeting on Optical Science and Technology, Vol. 4792, pp.173-184, July 2002.

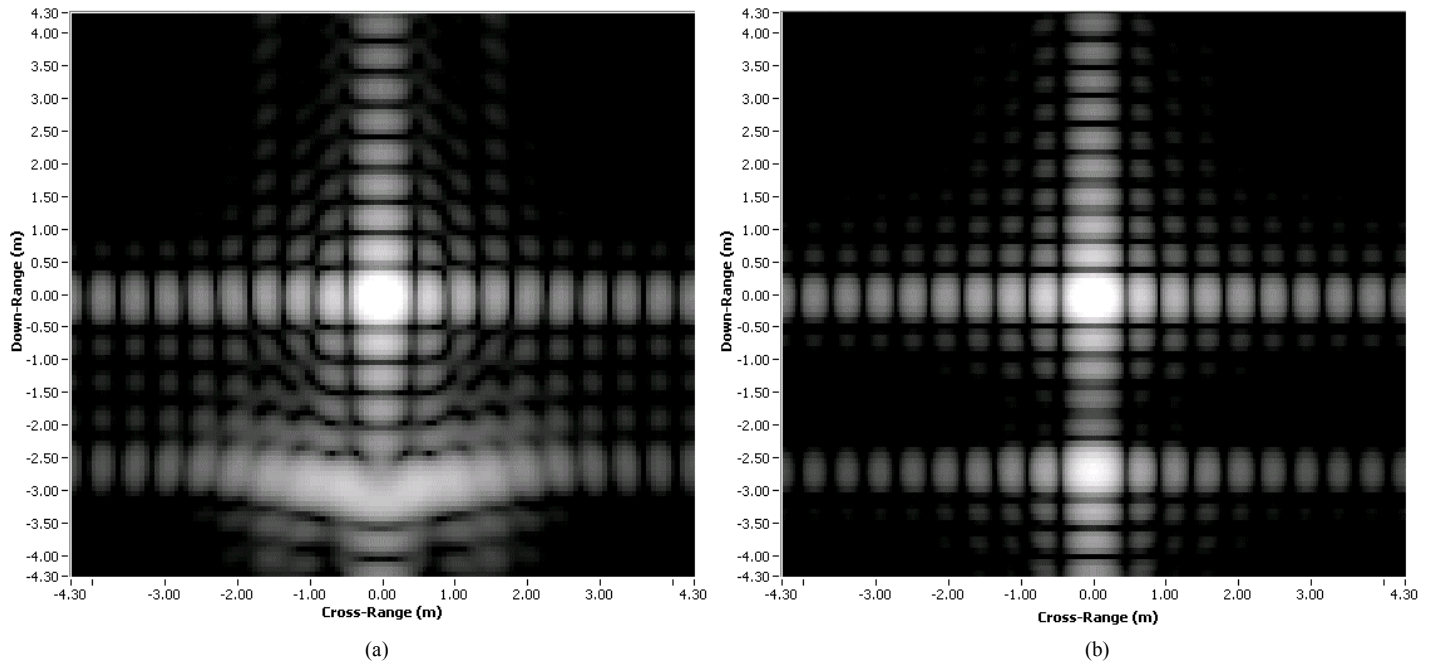


Fig. 5. Imagery of simulated data collections. (a) FGA (b) planar

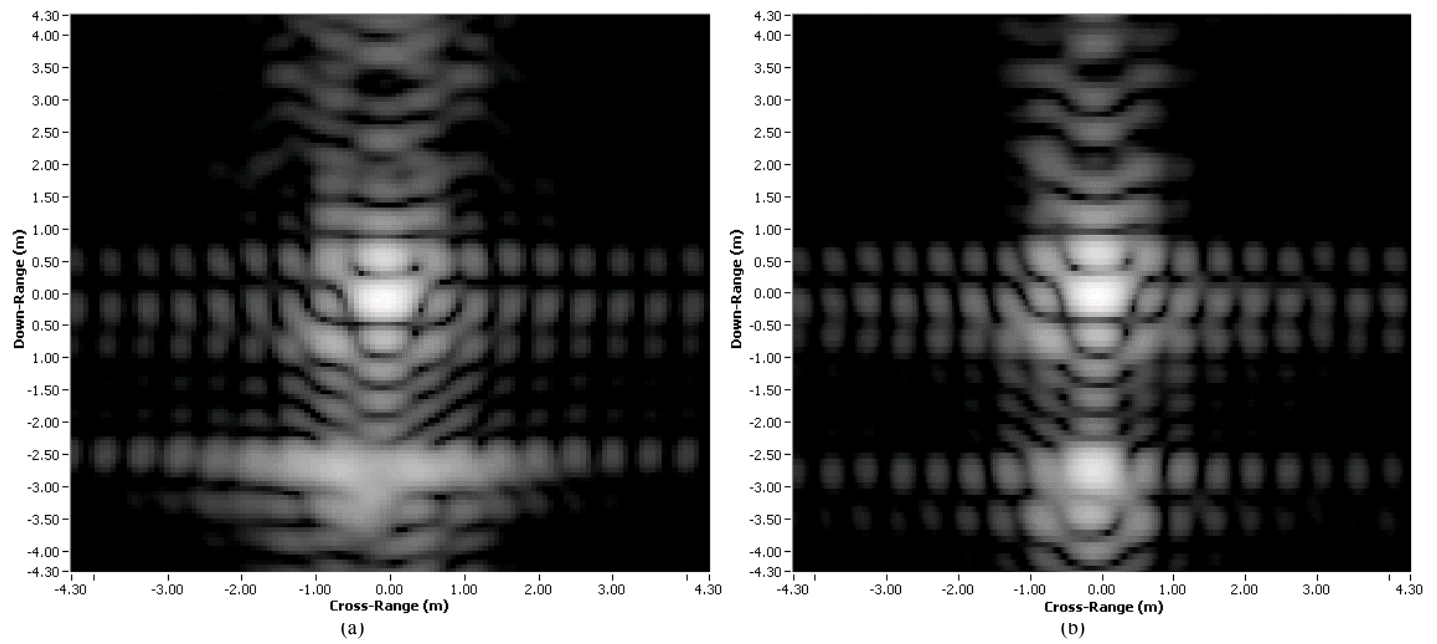


Fig. 6. Imagery of instrumented data collections. (a) FGA (b) planar